

Suppressing vortex generation in ferrofluidic Couette flow via alternating magnetic fields

Sebastian A. Altmeyer

Castelldefels School of Telecom and Aerospace Engineering, Universitat Politècnica de Catalunya, 08034 Barcelona, Spain

ARTICLE INFO

Keywords:

Ferrofluids
Rotating flows
Taylor–Couette flow
Suppressing vortex generation
Alternating magnetic field

ABSTRACT

We illustrate how an alternating magnetic field can restrict and suppress the generation of vortex formation in ferrofluidic Couette flow. Therefore, the initial rotating outer cylinder (inner cylinder at rest) is brought to an abrupt stop, which results in the generation of more complex vortex dynamics in the system, evolving out of the initially fully laminar flow regime. The generated vortex flow structures appear to be axisymmetric Taylor vortices. Different stages during the spin-down process are described and characterised through dynamic quantities, such as the kinetic energy, cross-flow energy, and angular velocity flux. The presence of an alternating magnetic field modifies these dynamics during the spin-down, which is mainly dominated by the modulation amplitude of the alternating field. While moderate modulation amplitudes tend to minimise the vortex formation, i.e. weaken the flow dynamics, large modulation amplitudes suppress any vortex formation. The driving frequency only has a minor effect in general, but may allow to select between different flow pattern within the process.

1. Introduction

To date, flow control is one of the key challenging tasks, both from a pure theoretical perspective and in particular with a focus on industrial applications. Rotating flows are a common choice to study the control in fluid dynamic problems. Here, the Taylor–Couette system (TCS) [1], the fluid flow contained in the annular gap between two, vertical and independent moving concentric cylinders, has been proven to be a very successful prototypical model system to understand such fundamental concepts in hydrodynamics. Numerous works have provided deeper insight into topics, such as global non-linear dynamics, bifurcation theory, pattern formation, [2–9], and eventually the transition towards turbulence [2,5,10].

Most commonly, such flow control is introduced via time-periodic forcing [11–20]. In the TCS with classical Newtonian fluid, this is frequently realised by the (axial or azimuthal) oscillation of one or both cylinders. Other choices are the pulsation of an axial imposed through flow and the application of a radial through flow (or both combined), with the latter requiring porous cylinder walls. In all these examples, such applied forcing requires a modification in the physical boundary conditions.

Instead, magnetic fluids, i.e. ferrofluids [21], offer an alternative method to realise such a periodic forcing. The great advantage lies in the fact that the forcing can be introduced *directly* into the system via a periodic modulation of the external magnetic field [22,23].

In TCS, the problem of an abrupt stoppage of the cylinder rotation has been addressed as a way to study the instabilities of an unsteady circular Couette flow (CCF). However, the number of works [24–26] on this topic is rare and the most common scenario has been considered. It is the case in which both cylinders were initially in solid body rotation from which then (in most cases) the outer one is stopped while the inner one remains in motion. With this setup, no final decay can be observed as energy is still introduced to the flow through the persisting rotation of the inner cylinder. As a result, depending on the rotation speed of the inner cylinder, the final state can be either the Taylor vortex flow (TVF), CCF, or even turbulence.

In the present work, we analyse the flow dynamics in the ferrofluidic TCS considering infinite (axial periodic) cylinders with moderate gap size (radii ratio $r_i/r_o = 0.8$) and inner cylinder permanent at rest. The numerical experiment starts at the temporal instant $t = 0$, when the initially constant rotation of the outer cylinder is abruptly stopped. Following this event, a transient, unsteady, dynamic flow evolves, referred to here as a spin-down phase. We observe the generation of a centrifugally unstable flow region starting near the outer cylinder, which eventually leads to the formation of axisymmetric, toroidally orientated, vortex patterns, i.e. Taylor vortices (TVF). During the whole spin-down process, various TVFs (with different numbers of vortex pairs) and transitions between them are found within the annulus. We investigate the flow dynamics during the spin-down in detail, when

E-mail address: sebastian.andreas.altmeyer@upc.edu.

<https://doi.org/10.1016/j.euromechflu.2023.11.007>

Received 18 May 2023; Received in revised form 14 November 2023; Accepted 17 November 2023

Available online 20 November 2023

0997-7546/© 2023 The Author(s). Published by Elsevier Masson SAS. This is an open access article under the CC BY license (<http://creativecommons.org/licenses/by/4.0/>).

alternating magnetic fields with different modulation amplitudes and frequencies are present, using a modified Niklas approach [22,27]. Therefore, various quantities, such as kinetic energy, cross-flow energy, mode contributions, and angular velocity flux, are considered. The modulation amplitude is found to be the dominant parameter to limit the flow dynamics, while the modulation frequency only plays a minor role, but may allow between different flow structures.

The paper is organised as follows. In Section 2, the system setting and methodology are presented together with the governing equations. The results are described and discussed in Section 3. Finally, Section 4 presents the summary and conclusion together with a future outlook.

2. System setting and parameters

2.1. Governing equations

The Taylor–Couette system (TCS) consists of two concentric, independently rotating cylinders. For the present study, the inner cylinder of radius r_i rotates initially at ω_i , while the outer cylinder of radius r_o is held at rest. Although knowing that the Ekman vortices play a crucial role in the dynamics of TCS, the present work has to be seen as a first study of such vortex suppressing, and therefore, we consider periodic boundary conditions in the axial direction with periodicity length λ and no-slip boundary conditions on the cylinder walls. Finite size systems will be studied in future works. The system is described as using a cylindrical polar coordinate system (r, θ, z) with a velocity field (u, v, w) . The radius ratio of the cylinders is set to $r_i/r_o = 0.8$, and the axial periodicity is set to $\lambda/(r_o - r_i) = 4$. The gap between the cylinders is filled with a viscous, incompressible, isothermal ferrofluid (APG933 [28,29]).

To realise a periodic forcing in the system, we apply a sinusoidal modulation signal to the external magnetic field, which is orientated parallel to the system symmetry (z) axis, uniform in space and harmonic in time $\mathbf{H}_z = [H_S + H_M \sin(\Omega_H t)]\mathbf{e}_z$ [22,23]. It is important to mention that such a *pure* axial-oriented magnetic field does *not* change the basic system symmetry, only the stability thresholds are shifted [27,30,31].

The flow dynamics of a ferrofluid with kinematic viscosity ν and density ρ are governed by the incompressible Navier–Stokes equations, including magnetic terms, and the continuity equation. Using the gap $d = (r_o - r_i)$ as the length scale, the diffusion time $\tau_D = d^2/\nu$ as the time scale, scaling pressure with $\rho\nu^2/d^2$, and the magnetic field \mathbf{H} and the magnetisation \mathbf{M} with $(\rho/\mu_0)^{0.5}\nu/d$ (μ_0 is the magnetic constant, i.e., magnetic permeability of free space), the non-dimensionalised ferro-hydrodynamical equations of motion [22,32–34] are given as:

$$\begin{aligned} (\partial_t + \mathbf{u} \cdot \nabla)\mathbf{u} - \nabla^2\mathbf{u} + \nabla p &= (\mathbf{M} \cdot \nabla)\mathbf{H} + \frac{1}{2}\nabla \times (\mathbf{M} \times \mathbf{H}), \\ \nabla \cdot \mathbf{u} &= 0. \end{aligned} \quad (2.1)$$

The cylinders are no-slip with velocity boundary conditions $\mathbf{u}(r_i, \theta, z) = (0, 0, 0)$ and $\mathbf{u}(r_o, \theta, z) = (0, Re, 0)$, where the outer Reynolds numbers is $Re = \omega_o r_o d/\nu$, which is initially held constant at $Re = 1700$ before the abrupt stoppage at $t = 0$.

To solve Eq. (2.1), one needs an equation that describes the magnetisation of the ferrofluid. Here we consider the equilibrium magnetisation of an unperturbed state, in which homogeneously magnetised ferrofluid is at rest, and the mean magnetic moment is orientated in the direction of the magnetic field; we have $M_{eq} = \chi H$. The magnetic susceptibility χ of the ferrofluid can be approximated with the Langevin formula [35], where we assume an initial value 0.9 and use a linear magnetisation law. Further, we consider the near equilibrium approximations of Niklas with small deviations $\|M - M_{eq}\|$ and small magnetic relaxation time $\tau: |\nabla \times \mathbf{u}|, \tau \ll 1$. A detailed description of the elimination process can be found in the Appendix in [22].

By using a modified Niklas approach [22,27,30,34] the effect of the magnetic field and the magnetic properties of the ferrofluid on

the velocity field can be characterised by a single (time-dependent) parameter:

$$s_z(t) = s_{z,S} + s_{z,M} \sin(\Omega_H t), \quad (2.2)$$

with $s_{z,S}$ being the *static contribution* of the driving $s_{z,M}$ the *modulation amplitude*, and Ω_H the *modulation frequency*. The exact procedure of how to solve the ferro-hydrodynamical equations of motion (2.1) is explained in detail in earlier works [22,23,36].

2.2. Numerics

Considering the near equilibrium approximation by Niklas [27], the magnetisation in the ferro-hydrodynamical equations of motion (2.1) can be eliminated, and the equations are solved by combining a standard, second-order, finite-difference scheme in (r, z) with a spectral decomposition in θ and (explicit) time splitting [22,30,33]. The variables can be expressed as follows:

$$f(r, \theta, z, t) = \sum_{m=-m_{\max}}^{m_{\max}} f_m(r, z, t) e^{im\theta}, \quad (2.3)$$

where f denotes one of the variables $\{u, v, w, p\}$. For the parameter regimes considered, the choice $m_{\max} = 16$ provides adequate accuracy. We use a uniform grid with spacing $\delta r = \delta z = 0.02$ and time steps $\delta t < 1/3800$.

For diagnostic purposes, we also evaluate the complex mode amplitudes $f_{m,n}(r, t)$, obtained from a Fourier decomposition in the axial direction:

$$f_m(r, z, t) = \sum_n f_{m,n}(r, t) e^{inkz}, \quad (2.4)$$

where $k = 2\pi d/\lambda$ is the axial wavenumber.

2.3. Nomenclature

Here we investigate flow structures in a (relatively) short periodic annulus with axial periodicity length $\Gamma = 4$. A common feature shared by all flow structures evolving during spin-down is that the axisymmetric Fourier mode associated with the azimuthal wavenumber, $m = 0$ (Eq. (2.3)), is dominant. Thus, the resulting flow states correspond to toroidally closed solutions. With the stoppage of the outer cylinder, the corresponding laminar boundary layer undergoes a primary centrifugal instability. This results in the formation of coherent (Taylor) rolls identifying the Taylor vortex flow (TVF). Taylor vortex flow with various different numbers of vortex pairs are found, which will be distinguished by an index i characterising the corresponding number of vortex pairs. For instance, TVF₅ identifies a TVF with 5 pairs of Taylor rolls, which in total means the presence of 10 vortices within the bulk [identified by a dominant mode amplitude $a_{0,5}$ (Eq. (2.4))]. Variation in the number of vortex pairs results in transitions (in quite a short amount of time) between different TVFs. It is worth mentioning, that the dynamics of the TVFs detected here are different to other similar-looking flow states that can be found in the finite TCS. These are stationary, non-propagating vortex states [37], with different numbers of vortices present in the annulus as well as non-stationary propagating vortex states [36,38–40]. The latter, time-dependent states, have natural, intrinsic axial dynamics, also *without* any external driving force.

3. Results

3.1. Evolving flow dynamics

We start with the flow dynamics evolving after the abrupt stop (at $t = 0$) of the outer cylinder rotation in the absence of any magnetic field. Therefore, Fig. 1 illustrates space–time plots of the radial velocity $u(r = r_i + d/2, \theta, z)$ (at mid-gap) and azimuthal vorticity $\eta = \partial_z u - \partial_r v$,

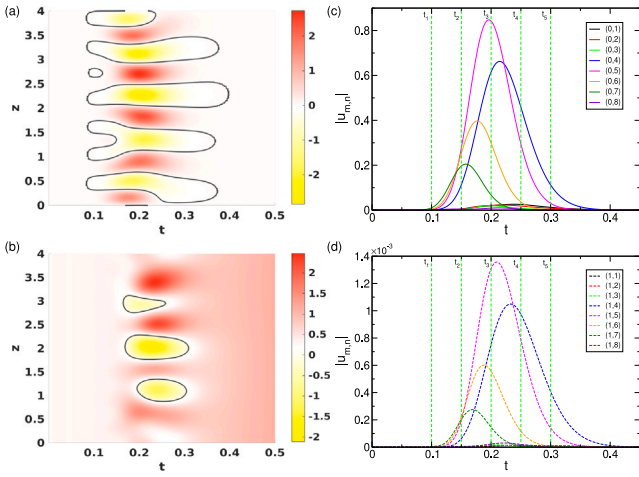


Fig. 1. Flow dynamics evolving with time t during the spin-down in the absence of a magnetic field ($s_{z,M}(t) = 0$). Shown here are space–time plots of the radial velocity (a) $u(r = r_i + d/2, \theta, z)$ and azimuthal vorticity (b) $\eta(r = r_i, \theta, z)$ (red (dark gray) and yellow (light gray) correspond to positive and negative values). Dominant mode amplitudes $|u_{m,n}|$ (cf. Eq. (2.4)) of the radial velocity field at mid-gap contributed from the (c) axisymmetric modes $(0, n)$ and (d) non-axisymmetric modes $(1, n)$. The time steps $t_i, i \in \{1, 5\}$ for which snapshots are shown in Fig. 4 are represented as green dashed lines. (The amplitudes of all modes with higher azimuthal wavenumbers, $m \neq 0$, are several orders smaller and do not play a role in the evolving flow dynamic (Fig. 1) and therefore, are not shown hereafter.) Note the different scaling in (c, d).

here $\eta(r = r_i, \theta, z)$ (at the inner cylinder), together with time series of mode amplitudes $|u_{m,n}|$ of the radial velocity field at mid-gap, contributed from the modes (m, n) as indicated. It is worth recalling that the initial state at $t = 0$ is given by the CCF. It takes about 0.083 (diffusion times) before one observes the formation of any vortex structures in the bulk. Here, an initial TVF₇ state with dominant toroidal flow dynamics including a total of 14 vortices (axial wavelength $\lambda = 0.286$ wavenumber $k = 21.99$) is formed. This flow evolves and transition very fast into other TVFs due to the elimination of vortex pairs. To be precise, the initial TVF₇ first transfers into TVF₆ ($\lambda = 0.333, k = 18.849$) at $t \approx 0.118$, followed by TVF₅ at $t \approx 0.148$ ($\lambda = 0.4, k = 15.708$) towards TVF₄ at $t \approx 0.238$ ($\lambda = 0.5, k = 12.566$). The latter, TVF₄, persists in the system the longest before it vanishes over a very short period from $t \approx 0.368$ over a sequence of flow states, TVF₄ → TVF₆ → TVF₂, before eventually at $t \approx 0.4$, all complex flow dynamics in the bulk disappear. Thus, the overall persistence time in which any TVFs are present in the bulk is $t_{\text{pers}} \approx 0.317$. Generally, the space–time plots of η at the inner cylinder wall feature in fewer dynamics than the corresponding ones at mid-gap. Moreover, any dynamics also appears significant later ($t \approx 0.16$), as the information and evolution of the flow structures have to travel from its origin at the (former) rotating outer cylinder through the bulk towards the inner cylinder.

Starting with CCF at $t = 0$, all radial mode amplitudes $|u_{m,n}|$ (Fig. 1(c, d)) grow from zero and become significant with the formation of the Taylor vortices. Thereby, the dominant mode dictates the corresponding TVF state. For instance, at $t \approx 0.2$, the mode amplitude $u_{0,5}$ (cf. Eq. (2.4)) is dominant, characterising TVF₅ with 5 pairs of vortices, indicating 10 vortices in the bulk as visible by the 10 contour lines in the space–time plot Fig. 1(a). All evolving flow dynamics illustrate toroidal flow structures dominated by the azimuthal $m = 0$ mode. The variation in the dominant mode amplitudes $|u_{m,n}|$ highlights the transition between the different TVFs. All higher azimuthal modes, $m \neq 0$, corresponding to higher azimuthal wavenumbers are at least 3 orders of magnitude smaller (Fig. 1(d)) and therefore negligible.

In the presence of an oscillating magnetic field with moderate field amplitude $s_{z,M} = 0.4$ (Fig. 2), we found qualitatively similar flow dynamics as in the absence of any magnetic field. However, the initial evolving TVF depends on the driving frequency Ω_H . While the

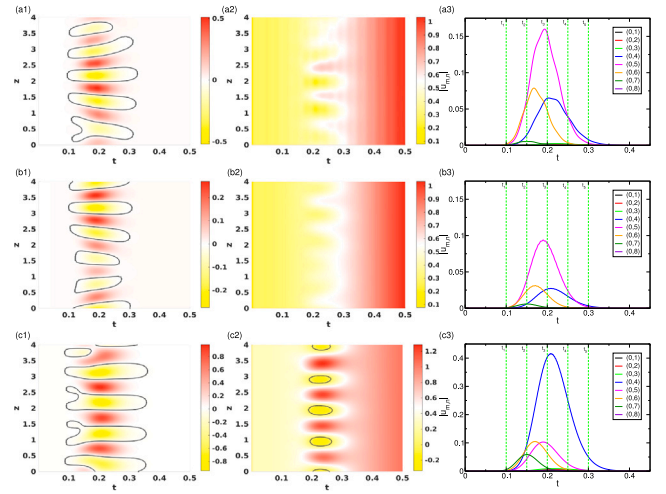


Fig. 2. Flow dynamics evolving with time t during spin-down for moderate field modulation amplitude $s_{z,M} = 0.4$. Shown here are space–time plots of (1) radial velocity $u(r = r_i + d/2, \theta, z)$, (2) azimuthal vorticity $\eta(r = r_i, \theta, z)$ (red (dark gray) and yellow (light gray) correspond to positive and negative values), and (3) corresponding dominant mode amplitudes $|u_{0,n}|$ of the radial velocity field at mid-gap (cf. Fig. 1). The modulation frequencies are (a) $\Omega_H = 100$, (b) $\Omega_H = 500$, and (c) $\Omega_H = 1000$. The time steps $t_i, i \in \{1, 5\}$, for which snapshots are shown in Fig. 4, are represented as green dashed lines. Note that the different scaling in (3) depends on Ω_H .

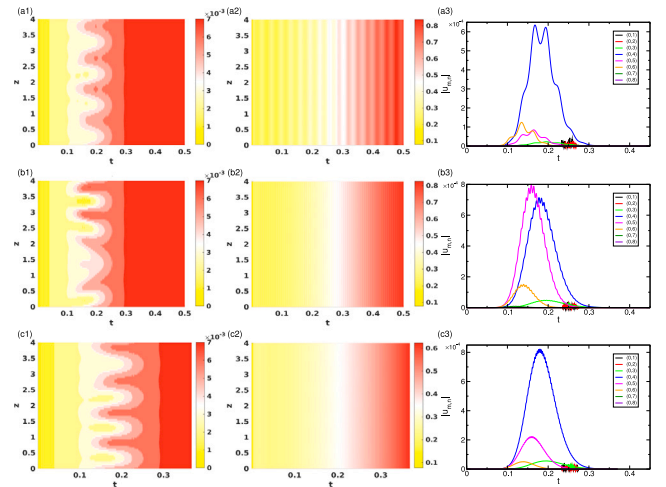


Fig. 3. As Fig. 2, but for strong field modulation amplitude $s_{z,M} = 1.0$. Note, that the mode amplitudes (3) $|u_{m,n}|$ are three orders of magnitude smaller than in the case of moderate field modulation amplitude $s_{z,M} = 0.4$.

number of formed Taylor vortices first decreases with increasing Ω_H from TVF₆ at $\Omega_H = 100$ to TVF₅ at $\Omega_H = 500$, for larger driving frequency $\Omega_H = 1000$, it is similar to the scenario without a magnetic field with the initial formation of TVF₇. Interestingly, for $\Omega_H = 100$ and $\Omega_H = 500$, the space–time plots of η at the inner cylinder wall (Fig. 2(a2, b2)) do not display any complex flow dynamics, which, in contrast, can be seen for $\Omega_H = 1000$ (Fig. 2(c2)). In general, all mode amplitudes $u_{m,n}$ are significantly smaller in comparison to the absence of an alternating magnetic field. For $s_{z,M} = 0.4$ all mode amplitudes $u_{m,n}$ become much smaller, only about 1/4 for $\Omega_H = 100$ and even only about 1/8 for $\Omega_H = 500$, compared to those with no magnetic field present. Meanwhile, the evolution with time of the modes (Fig. 2(3)) remains qualitatively similar as discussed before. As a result of the smaller modes, all flow structures appear weaker. However, for $\Omega_H = 1000$, the flow dynamics are enforced in comparison to the one observed at smaller driving frequencies $\Omega_H = 100$ and 500, visible also in

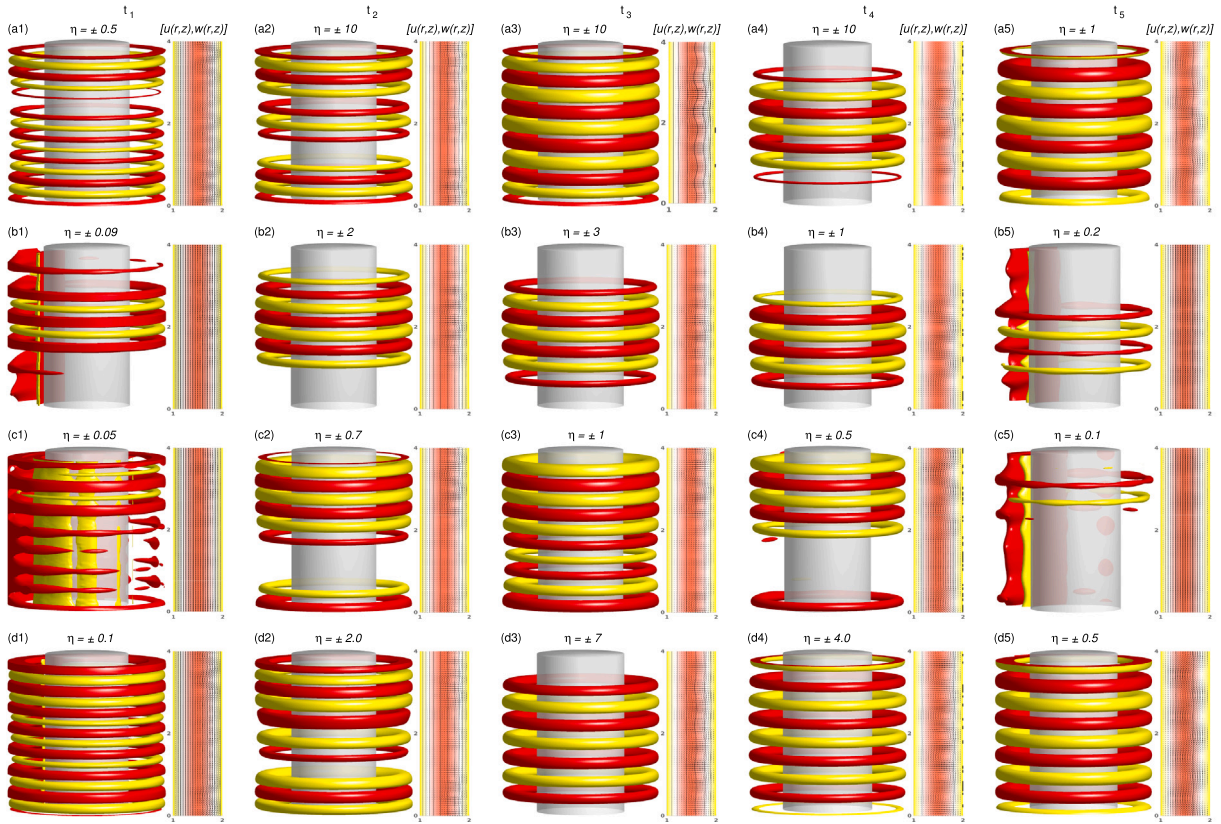


Fig. 4. Visualisation of the flow dynamics during spin-off. (a) In the absence of a magnetic field and with modulation amplitude $s_{z,M} = 0.4$, oscillation frequency (b) $\Omega_H = 100$, (c) $\Omega_H = 500$, and (d) $\Omega_H = 1000$. Shown here are isosurfaces of the azimuthal vorticity η [red (dark gray) and yellow (light gray) colors correspond to positive and negative values] [left panel], together with the vector plot $[u(r,z), w(r,z)]$ of the radial and axial velocity components (including the azimuthal vorticity) [right panel]. Time steps t_i , $i \in \{1, 5\}$ are highlighted by dashed green lines in Figs. 1(c, d), and 2(c), respectively. (For larger modulation amplitude $s_{z,M} = 1$, no similar flow structures have been detected, as all complex flow dynamics are basically suppressed.) Note the different contour levels chosen in the different subplots.

the notably larger mode amplitudes (about 1/2 compared to those without a magnetic field). Consistently one also observes stronger flow dynamics at the inner cylinder wall. Further, for high $\Omega_H = 1000$, the dominant flow structure appears to be TVF₄, indicated by the dominance of $u_{0,4}$ (representing 4 vortex pairs). (The amplitudes of all modes with higher azimuthal wavenumbers, $m \neq 0$, are several orders smaller and do not play a role in the evolving flow dynamics (Fig. 1) and are therefore not shown here or hereafter.)

Applying an alternating field with an even larger modulation amplitude $s_{z,M} = 1$ (Fig. 3) results in further and much stronger modification in the flow dynamics. All vortex formation becomes suppressed and only the roots (backbone) of such a formation remain visible in the space–time plots $u(r, \theta, z)$ (Fig. 3(a)). At the inner cylinder any dynamics are absent, as the information, i.e. the perturbation introduced at the outer cylinder, simply does not reach the inner cylinder at all. This suppressing behaviour is also visible in the evolution in the mode amplitudes $u_{0,n}$ (Fig. 3(c)), which appear to be about a further 3 orders of magnitude smaller and thus below the level that any Taylor vortices can form.

Fig. 4 illustrates different visualisations of TVFs and transitions between them as they are found to appear during the spin-down process. The corresponding time steps are indicated by green dashed lines in Fig. 1(c, d) and Fig. 3(c), respectively. The former described the weakening effect of the flow dynamics within the different TVFs, indicated by the decrease in the value η , for which the isosurfaces are presented. The larger the number, the larger the corresponding vortex structure. Note, that for larger modulation amplitude $s_{z,M} = 1$, all complex dynamics are mainly suppressed and therefore no similar flow structures have been found.

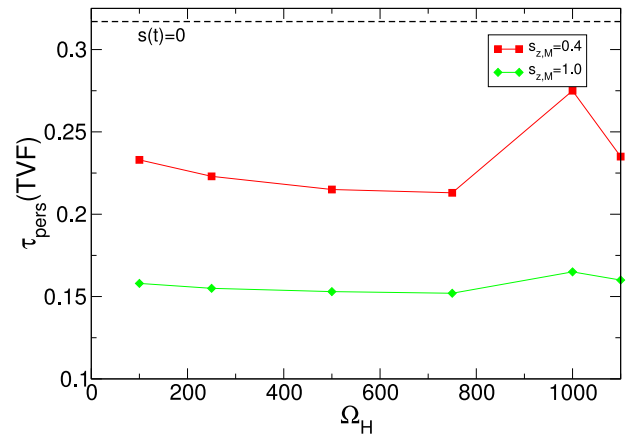


Fig. 5. Variation with frequency, Ω_H , for the persistence time $\tau_{\text{pers}}(\text{TVF})$ of TVFs within the bulk for $s_{z,M} = 0.4$ and (b) $s_{z,M} = 1.0$ (horizontal dashed line illustrates the scenario in the absence of a magnetic field). Note, that for $s_{z,M} = 1.0$, $\tau_{\text{pers}}(\text{TVF})$ is a combined approximation, as no full TVFs appear (see text for further details).

If an alternating magnetic field is present, a common observation is that any complex flow dynamics appears later after the abrupt stoppage, and at the same time also disappears earlier in comparison to the scenario without the presence of any magnetic field. Together, they result in a shrinking and squeezing in the persistence time $\tau_{\text{pers}}(\text{TVF})$ for which TVFs are present within the bulk (Fig. 5). Note that for

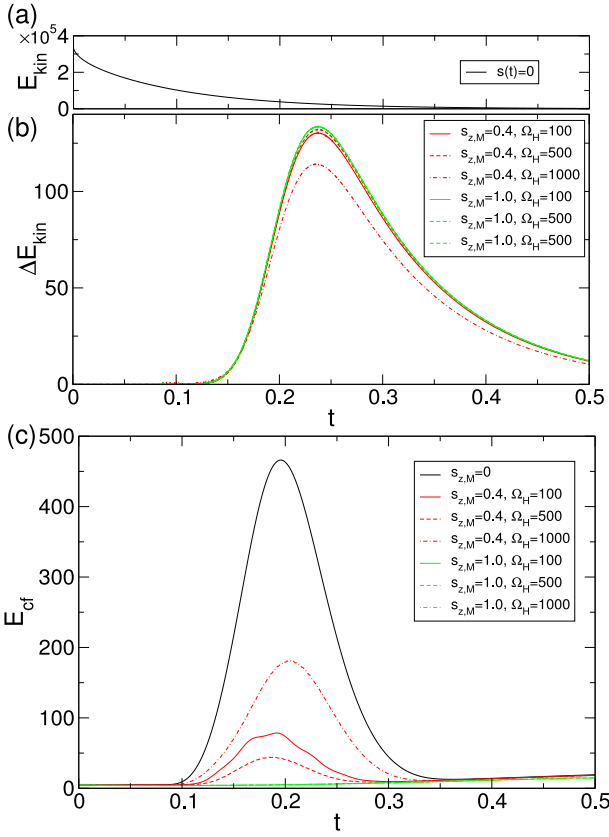


Fig. 6. Time series of (a) total kinetic energy E_{kin} for $s_z(t) = 0$ and (b) differences $\Delta E_{kin} = E_{kin}[s_z(t)] - E_{kin}[s_z(t) = 0]$ in comparison with alternating fields for moderate modulation amplitude $s_{z,M} = 0.4$, and for large modulation amplitude $s_{z,M} = 1.0$ at different frequencies $\Omega_H = 100, 500, 1000$ as indicated. (c) Time series of the corresponding cross-flow energy E_{cf} .

$s_{z,M} = 1.0$, no fully developed TVFs appear, only the roots of such flows can be detected; here $\tau_{pers}(TVF)$ is a combined approximation based on the space–time plots (Fig. 2(2)), together with the variation in the time-evolution of the dominant mode amplitudes $|u_{0,n}|$ (Fig. 2(3)). For any modulation amplitude, with increasing driving frequency Ω_H , the persistence time $\tau_{pers}(TVFs)$ first decreases before for high Ω_H , and $\tau_{pers}(TVFs)$ increases. However, $\tau_{pers}(TVFs)$ always remains below the corresponding time $\tau_{pers}^{s_z(t)=0}(TVFs)$ in the absence of any magnetic field. One possible speculation for this detected non-monotonous behaviour may be the appearance of resonance effects, which could be supported by similar recent observations [23]. The decrease in $\tau_{pers}(TVF)$ for $\Omega_H = 1100$ (Fig. 5) can be seen as another indicator for this speculation.

3.2. Kinetic energy and cross-flow energy

After the qualitative analysis of the evolving flow dynamics during the spin-down, we will now focus on different quantitative measures.

As a global quantity to characterise the flow, we use the following modal kinetic energy

$$E_{kin} = \sum_m E_m = \frac{1}{2} \int_0^{l/2} \int_{-l/2}^{l/2} \int_{r_i}^{r_o} \mathbf{u}_m \mathbf{u}_m^* r dr dz d\theta, \quad (3.1)$$

where \mathbf{u}_m (\mathbf{u}_m^*) is the m th (complex conjugate) Fourier mode of the velocity field (Eq. (2.3)).

Further, to study the flow characteristics, we also consider the cross-flow energy [41],

$$E_{cf}(t) = \langle u_r^2 + u_z^2 \rangle_{r,\theta,z}. \quad (3.2)$$

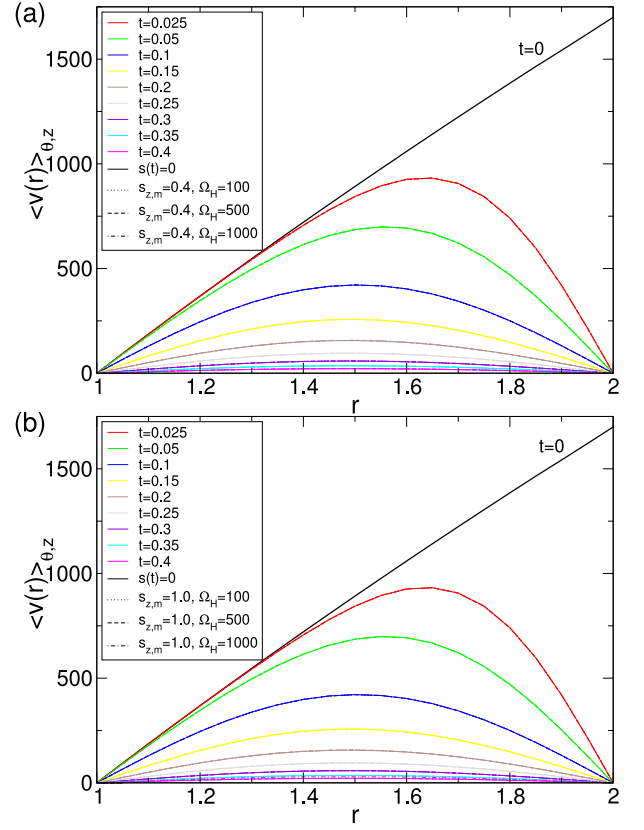


Fig. 7. Radial decay process in the mean (averaged) azimuthal velocity $\langle v(r) \rangle_{\theta,z}$ for times t as indicated for (a) $s_{z,M} = 0.4$ and (b) $s_{z,M} = 1.0$. The curves for different driving frequencies, Ω_H , fall together and are indistinguishable.

Although the variation with time of the total kinetic energy E_{kin} (Fig. 6(a)) is similar, one can observe differences if an alternating magnetic field is present. An alternating magnetic field slightly decreases E_{kin} , as visible in the positive values $\Delta E_{kin} = E_{kin}(s_z(t)) - E_{kin}(s_z(t) = 0)$ (Fig. 6(b)). While for moderate mode amplitude $s_{z,M} = 0.4$ and small to moderate frequencies $\Omega_H = 100$ and 500 , ΔE_{kin} increases, for very high oscillation frequency $\Omega_H = 1000$, one observes an opposite behaviour with a clear decrease in ΔE_{kin} . Larger modulation amplitude results in an increase in the differences ΔE_{kin} . Notably, for $s_{z,M} = 1$ the curves for different Ω_H all fall together, and therefore are indistinguishable.

In contrast to E_{kin} (ΔE_{kin}) the corresponding cross-flow energy $E_{cf}(t)$ within the system decreases in comparison with to the scenario in absence of any field (Fig. 6(c)). As seen for E_{kin} also $E_{cf}(t)$ is indistinguishable for large modulation amplitude $s_{z,M} = 1$. The value remains very small confirming the former already mentioned fact that virtual now more complex flow dynamics, e.g. the formation of Taylor vortices appears. Meanwhile, for $s_{z,M} = 0.4$ and $\Omega_H = 1000$, E_{cf} increases in comparison to smaller driving frequencies $\Omega_H = 100$ and 500 .

Another important aspect is the decay of the azimuthal velocity profile $\langle v(r) \rangle_{\theta,z}$ as a function of time. Fig. 7 shows the azimuthal velocity profile at different time steps (see also Figs. 1 and 2). Here, the azimuthal velocity is averaged axially and at each instant of time. A few selected time-steps were chosen to present the evolution of the flow dynamics. The initial profile at $t = 0$ is the analytic laminar profile, the CCF profile. Then, after the abrupt stoppage of the outer cylinder, the next profiles ($t = 0.025$ and $t = 0.05$) remain close to the Couette flow in the first half of the gap ($1 \lesssim r \lesssim 0.5$), then reach a maximum value within the outer half ($r \approx 1.6 - 1.7$), and decrease towards zero at the outer cylinder wall. For the following time steps, the profiles remain

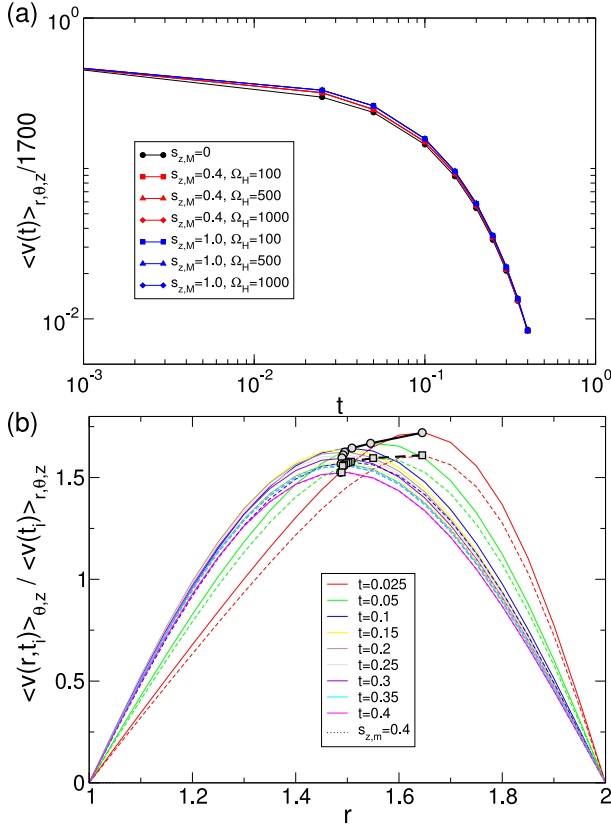


Fig. 8. (a) Total decay process of mean (averaged) azimuthal velocity $\langle v(t) \rangle_{r,\theta,z}$ versus time t for $s_{z,M}$ and Ω_H , as indicated. (b) Radial profile of mean (averaged) azimuthal velocity (cf. Fig. 7(a), modulation amplitude $s_{z,M} = 0.4$) normalised with its spatial mean value, $\langle v(r,t) \rangle_{\theta,z} / \langle v(t) \rangle_{r,\theta,z}$. The solid line with circles and dashed line with squares indicate the variation with time in the maxima in the corresponding profiles.

qualitatively the same, while continuously flattening, i.e. becoming smaller. Thereby, the maxima in the profiles remain located in the centre region (at mid-gap, $r \approx 1.5$) of the bulk. For $t = 0.4$ the profile almost reaches zero.

Fig. 8(a) presents the evolution of the mean azimuthal velocity, $\langle v(t) \rangle_{r,\theta,z}$, concerning time. During the decay, the mean azimuthal velocity does not follow a single power law, whereby the curves for different mode amplitudes remain the same qualitatively, but differ in their quantity. However, the curves for the same modulation amplitude $s_{z,M}$, but different oscillation frequencies Ω_H are indistinguishable. In agreement with the former observation, with increasing $s_{z,M}$, the kinetic energy, E_{kin} , increases while the cross-flow energy, E_{cf} , decreases. Here the azimuthal velocity $\langle v(t) \rangle_{r,\theta,z}$ becomes largest with increasing $s_{z,M}$. Fig. 8(b) presents the self-similarity picture for the radial profile azimuthal velocity during the spin-down process for moderate modulation amplitude $s_{z,M} = 0.4$. Velocity profiles were averaged axially and over time, and then normalised with their spatial average (cf. Fig. 7(a)). Although the maxima in the profiles are initially different, i.e. they are smaller in the presence of an alternating field, they move similarly in a short amount of time (independent of the field) towards the centre region $r \approx 1.5$. Thereby, the corresponding maxima also approach each other in magnitude, before they are almost identical for $t = 0.4$.

3.3. Momentum flux and cross-flow energy

The conserved transported quantity between two cylinders can be expressed in terms of the angular velocity flux:

$$J_\omega = r^3 \langle (uv/r) \rangle_{A(r)} - v \partial_r \langle v/r \rangle_{A(r)} \quad (3.3)$$

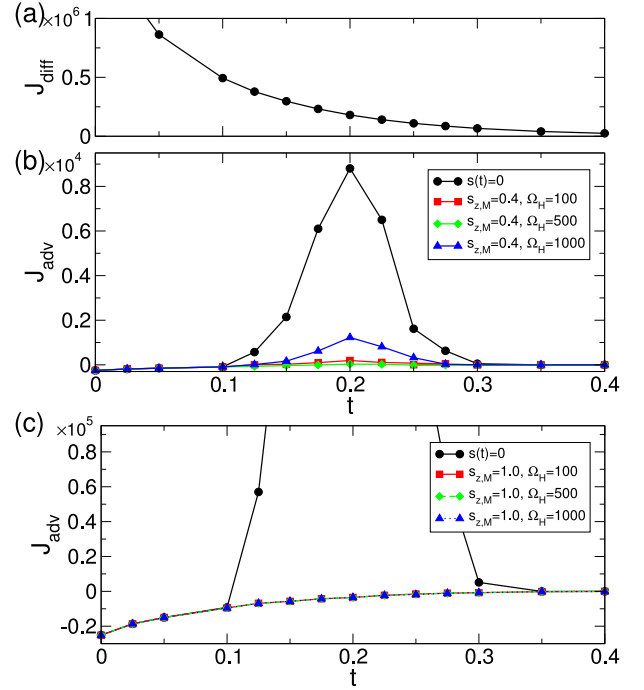


Fig. 9. Variation with time t in the two contributions J_{diff} and J_{adv} of the angular velocity flux J_ω (Eq. (3.3)). (a) J_{diff} with and without magnetic field: the curves fall together. (b) $s_{z,M} = 0.4$, (c) $s_{z,M} = 1.0$. Note, the different scaling in (c) and that here also all curves for different frequencies Ω_H fall together.

$$= J_{diff} + J_{adv},$$

where $A(r)$ stands for the averaging over the surface of a concentric cylinder at radius r . The two contributions, $J_{diff} = r^3 \langle (uv/r) \rangle_{A(r)}$ standing for the averaged diffusive contribution, and $J_{adv} = -r^3 v \partial_r \langle v/r \rangle_{A(r)}$ for the advective contribution, are also called molecular transport [41]. The total angular velocity flux J_ω is dominated by the diffusive contribution J_{diff} , which is several orders of magnitude larger compared to the advective contribution J_{adv} . For both modulation amplitudes $s_{z,M} = 0.4$ and $s_{z,M} = 1.0$, no differences are visible in J_{diff} (Fig. 9), the curves lie on top of each other. On the other hand, such differences appear in J_{adv} (Fig. 9(b,c)).

For moderate modulation amplitude $s_{z,M} = 0.4$, one finds a qualitatively similar behaviour in J_{adv} as in the absence of an alternating field, whereby the contributions J_{adv} are notably smaller, at least one order of magnitude. Further, J_{adv} is different, depending on the driving frequency Ω_H , with the largest contribution appearing with the highest frequency $\Omega_H = 1000$. For large modulation amplitude $s_{z,M} = 1$, independent of the driving frequency Ω_H , basically any contribution in J_{adv} disappears, indicating the suppression of vortex formation.

To get a better understanding of the flow dynamics and evolution in the bulk, Fig. 10 illustrates the contributions J_{diff} and J_{adv} (Eq. (3.3)) versus the radius r for different time steps t_i as indicated (Fig. 9(a)). Note that here we only present results for $s_{z,M} = 0.4$, and we avoid presenting similar results for $s_{z,M} = 1$, as any vortex formation is suppressed. The corresponding values of J_{adv} are more than 2 orders of magnitude smaller compared to those for $s_{z,M} = 0.4$.

As mentioned before, the diffusive contribution J_{diff} is by far the dominant one in the full momentum flux J_ω . This holds for any time step t_i . Moreover, virtually no difference can be found in the presence or absence of an alternating field (Fig. 10(a)), as all curves at the corresponding time t_i fall together. With increasing time t_i , the profiles $J_{diff}(r)$ continuously flatten out in the approach to reach zero, as seen in Fig. 9(a). Although, about 3 to 4 orders are of smaller magnitude, the profiles $J_{adv}(r)$ illustrate a clear maximum in the outer half of the bulk

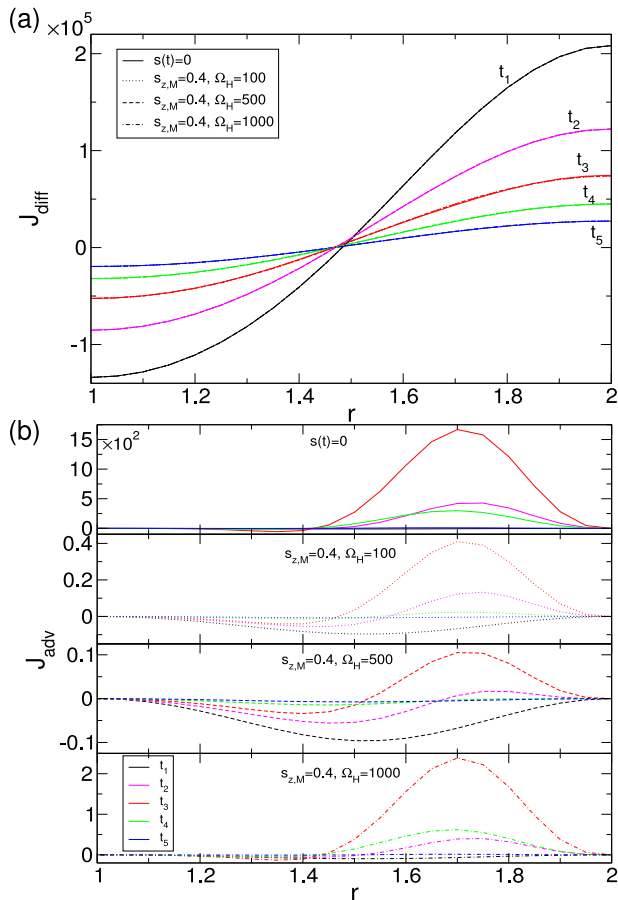


Fig. 10. Variation in the two contributions (a) J_{diff} and (b) J_{adv} (Eq. (3.3)) versus the radius r for five different time steps, t_i , $i \in \{1, 5\}$, as indicated in the absence of a field and moderate modulation amplitude $s_{z,M} = 0.4$.

($r \approx 1.7$) for time step t_3 , when the temporal generated TVF is present in the bulk. This holds similar for any modulation frequency Ω_H , whereby if an oscillating field is present, J_{adv} is a minimum of 2 orders of magnitude smaller (see ordinate axis in Fig. 10(b)) in comparison to the situation without any magnetic field.

4. Conclusion and discussion

In this study, we investigated the instantaneous stoppage of the outer cylinder rotation in the Taylor–Couette system (inner cylinder at rest at all time), considering a ferrofluid under the influence of alternating magnetic fields. With the initial presence of a pure laminar flow, such an abrupt stoppage leads to the generation, and consequently, the decay of vortex dynamics due to the absence of any further driving force. The reference scenario is given by the system in the absence of any field. The following process is observed here: the stoppage induces the generation of a centrifugally unstable flow region near the outer cylinder. This leads to the formation of an axisymmetric vortex flow pattern — Taylor vortices with different numbers of vortex pairs within the annulus. All evolving flow structures during the spin-down process are toroidally orientated with dominant azimuthal $m = 0$ modes, higher azimuthal modes $m > 0$ can be neglected. While the mean azimuthal velocity continuously decreases during the whole decay process, the growth of the vortices is accompanied by continuous re-adjustments as they grow and propagate towards the inner cylinder. Within this process the corresponding cross-flow energy E_{cf} increases, reaching a maximum at the time when the whole gap is filled with the axisymmetric flow, and decaying with the re-organisation of the flow structures.

Following the formation of the strongest structure the viscous diffusion is dominating the last phase with the transition over different TVFs, continuously reducing the number of vortex pairs, until eventually, all flow dynamics disappear in the bulk. It is worth mentioning that the cross-flow energy E_{cf} always remains smaller in comparison to the scenario in the absence of any magnetic field $s_z(t) = 0$. Besides E_{cf} shows a non-monotonous behaviour, an increase is found for the largest oscillation frequency $\Omega_H = 1000$ at fixed modulation amplitude $s_{z,M} = 0.4$. Based on recent findings [23], one can speculate that this originates in resonances in the system.

The presence of an alternating magnetic field has a direct effect on the evolving flow characteristics, and the flow dynamics in the system become limited. In the case of moderate modulation amplitude $s_{z,M} = 0.4$, the flow structures become weaker, i.e. the azimuthal vorticity within the Taylor vortices becomes smaller. However, similar flow dynamics can be found in the absence of a magnetic field, with the generation of TVFs and their decay in a sequence of transitions between different TVFs. Any variation in the driving frequency Ω_H mainly results in the formation of different dominant TVFs. Various characteristic quantities, such as mode amplitudes, and cross-flow energy, are found to be about 3 orders of magnitude smaller. In addition, the persistence time of the temporal evolving TVFs also becomes smaller when an alternating field is present.

For large modulation amplitude $s_{z,M} = 1.0$, the evolution and formation of any more complex flow dynamics, e.g. TVFs, are suppressed, and only the roots (backbone) of such dynamics remain as reminiscence observable in the system (various quantities are found to be about 6 orders of magnitudes smaller). For such large modulation amplitudes, any variation in the oscillation frequency, Ω_H is negligible.

This behaviour can be understood by and related to the total decay process of mean azimuthal velocity during the spin-down. With increasing modulation amplitude, the corresponding mean azimuthal velocity increases, in particular for the initial time after the abrupt stoppage, while at the same time, the kinetic energy decreases and the cross-flow energy increases. These processes together limit the possibility for any information (perturbation) to travel through the bulk, from the outer towards the inner cylinder. In addition, the persistence time for detected more complex flow dynamics, TVFs, is reduced.

Thus, an alternating magnetic field can control the flow after an abrupt stoppage of the outer cylinder rotation in TCS. Such a magnetic field suppresses (or at least minimises) the growing of the circular instability near the outer cylinder during the spin-down process. Therefore, it controls and mainly limits the effect of any enhanced mixing, if not desired, due to the suppression of any complex flow dynamics, here in particular the formation of Taylor vortices. Four key points for future studies are: first, the exploration of a wider parameter space. Second the effect on other, more complex flow structures, e.g. spirals, wavy vortices, etc. Third, the conditions when an oscillating magnetic field can be replaced by the time averaged value. Fourth, most important, the consideration of realistic, finite size system. Here, the omnipresent Ekman vortices may affect the whole dynamic. Besides this may provide valuable insight for industrial Taylor flow in reactors and other devices, i.e. Taylor reactor, centrifugal extractors, biological reactors, and filtration devices [42–44], just to name a few. Moreover, it remains to be seen, how this flow dynamics in combination with alternating magnetic fields will unfold at larger Reynolds numbers and here in particular for those when turbulence appears in the system. Experimental analysis is always valuable. However, numerical studies can provide ideas or hint at solutions.

Declaration of competing interest

The authors declare the following financial interests/personal relationships which may be considered as potential competing interests: Sebastian A. Altmeyer reports financial support was provided by Spain Ministry of Science and Innovation.

Data availability

Data will be made available on request.

Acknowledgements

S. A. is a Serra Hünter Fellow. This work has been supported by the Spanish Government under grant PID2019-105162RB-I00.

References

- [1] G.I. Taylor, Stability of a viscous liquid contained between two rotating cylinders, *Philos. Trans. R. Soc. Lond. A* 223 (1923) 289.
- [2] D. Coles, Transition in circular Couette flow, *J. Fluid Mech.* 21 (1965) 385.
- [3] C.A. Jones, Nonlinear Taylor vortices and their stability, *J. Fluid Mech.* 102 (1981) 249.
- [4] P. Chossat, G. Iooss, *The Couette-Taylor Problem*, Springer, Berlin, 1994.
- [5] C.D. Andereck, S.S. Liu, H.L. Swinney, Flow regimes in a circular couette system with independently rotating cylinders, *J. Fluid Mech.* 164 (1986) 155.
- [6] S. Chandrasekhar, *Hydrodynamic and Hydromagnetic Stability*, Dover, New York, 1981.
- [7] R.C. DiPrima, H.L. Swinney, Instabilities and transition in flow between concentric rotating cylinders in Hydrodynamic Instabilities and the Transition to Turbulence, in: *Topics in Applied Physics*, Vol. 45, Springer, Berlin, 1985.
- [8] R. Donnelly, Taylor–Couette flow: the early days, *Phys. Today* 44 (1991) 32.
- [9] R. Tagg, The Couette–Taylor problem, *Nonlinear Sci. Today* 4 (3) (1994) 1.
- [10] D. Ruelle, F. Takens, On the nature of turbulence, *Comm. Math. Phys.* 20 (1971) 167.
- [11] A. Ganske, T. Gebhardt, S. Grossmann, Modulation effects along stability border in Taylor–Couette flow, *Phys. Fluids* 6 (1994) 3823.
- [12] R.F. Donnelly, F. Reif, H. Suhl, Enhancement of hydrodynamic stability by modulations, *Phys. Rev. Lett.* 9 (1962) 363.
- [13] S. Carmi, J.I. Tustaniwskyj, Stability of modulated finite-gap cylindrical couette flow: linear theory, *J. Fluid Mech.* 108 (1981) 19.
- [14] C.F. Barenghi, C.A. Jones, Modulated Taylor–Couetter flow, *J. Fluid Mech.* 208 (1989) 127.
- [15] C.F. Barenghi, Computations of transitions and Taylor vortices in temporally modulated Taylor–Couette flow, *J. Comput. Phys.* 95 (1991) 175.
- [16] R.F. Donnelly, Experiments on the stability of viscous flow between rotating cylinders. III, Enhancement of stability by modulation, *Proc. R. Soc. Lond. Ser. A Math. Phys. Eng. Sci.* 281 (1964) 130.
- [17] F. Marques, J. Lopez, Spacial and temporal resonances in a periodically forced hydrodynamic system, *Physica D* 136 (2000) 340.
- [18] A.Y. Weisberg, I.G. Kevrekidis, A.J. Smits, Delaying transition in Taylor–Couette flow with axial motion of the inner cylinder, *J. Fluid Mech.* 348 (1997) 141.
- [19] B.T. Murray, G.B. McFadden, S.R. Coriell, Stabilization of Taylor–Couette flow due to time-periodic outer cylinder oscillation, *Phys. Fluids A Fluid Dyn.* 2 (1990) 2147.
- [20] H.C. Hu, R.E. Kelly, Effect of a time-periodic axial shear flow upon the onset of Taylor vortices, *Phys. Rev. E* 51 (1995) 3242.
- [21] R.E. Rosensweig, *Ferrohydrodynamics*, Cambridge University Press, 1985.
- [22] S. Altmeyer, On the ridge of instability in ferrofluidic Couette flow via alternating magnetic field, *Sci. Rep.* 11 (2021) 4705.
- [23] S.A. Altmeyer, Ferrofluidic wavy Taylor vortices under alternating magnetic field, *Phil. Trans. R. Soc. A* 381 (2023) 20220121.
- [24] K.R. Kohuth, G.P. Neitzel, Experiments on the instability of an impulsively-initiated circular Couette flow, *Exp. Fluids* 6 (1988) 199–208.
- [25] G.P. Neitzel, Marginal stability of impulsively initiated Couette flow and spin-decay, *Phys. Fluids* 25 (1982) 226.
- [26] G.P. Neitzel, S.H. Davis, Centrifugal instabilities during spin-down to rest in finite cylinders, numerical experiments, *J. Fluid Mech.* 102 (1981) 329.
- [27] M. Niklas, Influence of magnetic fields on Taylor vortex formation in magnetic fluids, *Z. Phys. B* 68 (1987) 493.
- [28] J. Embs, H.W. Müller, C. Wagner, K. Knorr, M. Lücke, Measuring the rotational viscosity of ferrofluids without shear flow, *Phys. Rev. E* 61 (2000) R2196.
- [29] The specifications for the ferrofluid APG933 are as follows: $\mu_0 M_s = 20mT$, $\eta = 500$ mPas, density $\rho = 1.09g/cm^3$, $\Phi_m = 3.3\%$, susceptibility $\chi = 0.9$, mean diameter of the particle's magnetic core 10 nm, thickness of the polymeric coating 2 nm.
- [30] S. Altmeyer, C. Hoffmann, A. Leschhorn, M. Lücke, Influence of homogeneous magnetic fields on the flow of a ferrofluid in the Taylor–Couette system, *Phys. Rev. E* 82 (2010) 016321.
- [31] M. Reindl, S. Odenbach, Influence of a homogeneous axial magnetic field on Taylor–Couette flow of ferrofluids with low particle–particle interaction, *Expts. Fluids* 50 (2011) 375.
- [32] H.W. Müller, M. Liu, Structure of ferrofluid dynamics, *Phys. Rev. E* 64 (2001) 061405.
- [33] S. Altmeyer, Ferrofluidic Couette flow in time-varying magnetic field, *J. Magn. Magn. Mater.* 552 (2022) 169205.
- [34] S. Altmeyer, Increasing flow complexity in time-dependent modulated ferrofluidic couette flow, *Fluid Dyn.* 57 (3) (2022) 387.
- [35] P. Langevin, Magnétisme et théorie des électrons, *Ann. Chem. et de Phys.* 5 (1905) 70–127.
- [36] S. Altmeyer, Propagating vortices in ferrofluidic Couette flow under magnetic fields - Part I: Axial and symmetry breaking transversal orientated fields, *J. Magn. Magn. Mater.* 527 (2021) 167769.
- [37] M. Heise, Ch. Hoffmann, Ch. Will, S. Altmeyer, J. Abshagen, G. Pfister, Co-rotating Taylor–Couette flow enclosed by stationary disks, *J. Fluid Mech.* 716 (2013) R4–1.
- [38] C. Hoffmann, S. Altmeyer, M. Heise, J. Abshagen, G. Pfister, Axisymmetric propagating vortices in centrifugally stable Taylor–Couette flow, *J. Fluid Mech.* 728 (2013) 458.
- [39] T. Ilzig, K. Stöckel, S. Odenbach, Experimental investigations on the effect of axial homogenous magnetic fields on propagating vortex flow in the Taylor–Couette system, *Materials* 12 (2019) 4027.
- [40] S. Altmeyer, Propagating vortices in ferrofluidic Couette flow under magnetic fields - Part II: Oblique orientated fields, *J. Magn. Magn. Mater.* 527 (2021) 167788.
- [41] H.J. Brauckmann, B. Eckhardt, Intermittent boundary layers and torque maxima in Taylor–Couette flow, *Phys. Rev. E* 87 (2013) 033004.
- [42] J. Zhu, D. Liu, C. Tang, C.Q. Chao, C.L. Wang, Study of slit wall aspect ratio effect on the Taylor vortex flow, *J. Eng. Thermophys.* 37 (2016) 1208–1211.
- [43] J. Yin, X. Liu, C. Zhou, Z. Zhu, Analysis and measurement of mixing flow field on side wall of large-scale mixing tank, *Chem. Eng.* 49 (2021) 73–78.
- [44] S. Altmeyer, Effect of axial and radial flow on the hydrodynamics in a Taylor reactor, *Fluids* 7 (2022) 336.